Biogeosciences Discuss., 11, 12631–12671, 2014
www.biogeosciences-discuss.net/11/12631/2014/
doi:10.5194/bgd-11-12631-2014

Biogeosciences
Discussions
Open Access

Estimates of micro-, nano-, and picoplankton contributions to particle export in the northeast Pacific

B. L. Mackinson[1], **S. B. Moran**[1], **M. W. Lomas**[2], **G. M. Stewart**[3], and **R. P. Kelly**[1]

[1]Graduate School of Oceanography, University of Rhode Island, Narragansett, RI 02882, USA
[2]Bigelow Laboratory for Ocean Sciences, East Boothbay, Maine 04544, USA
[3]Queens College and Graduate Center, City University of New York, Flushing, NY 11367, USA

Received: 23 July 2014 – Accepted: 31 July 2014 – Published: 27 August 2014

Correspondence to: B. L. Mackinson (bmackinson@my.uri.edu)

Published by Copernicus Publications on behalf of the European Geosciences Union.

Abstract

The contributions of micro-, nano-, and picoplankton to particle export were estimated from measurements of size-fractionated particulate ^{234}Th, organic carbon, and phytoplankton indicator pigments obtained during five cruises between 2010 and 2012 along Line P in the subarctic northeast Pacific Ocean. Sinking fluxes of particulate organic carbon (POC) and indicator pigments were calculated from ^{234}Th–^{238}U disequilibria and, during two cruises, measured by sediment trap at Ocean Station Papa. POC fluxes at 100 m ranged from 0.65–7.95 mmol m^{-2} d^{-1}, similar in magnitude to previous results at Line P. Microplankton pigments dominate indicator pigment fluxes (averaging 69 ± 19 % of total pigment flux), while nanoplankton pigments comprised the majority of pigment standing stocks (averaging 64 ± 23 % of total pigment standing stock). Indicator pigment loss rates (the ratio of pigment export flux to pigment standing stock) point to preferential export of larger microplankton relative to smaller nano- and picoplankton. However, indicator pigments do not quantitatively trace particle export resulting from zooplankton grazing, which may be an important pathway for the export of small phytoplankton. These results have important implications for understanding the magnitude and mechanisms controlling the biological pump at Line P in particular, and more generally in oligotrophic gyres and high-nutrient, low-chlorophyll regions where small phytoplankton represent a major component of the autotrophic community.

1 Introduction

Phytoplankton community structure exerts an important influence on the strength and efficiency of the biological pump (Michaels and Silver, 1988; Boyd and Newton, 1999; Thibault et al., 1999; Brew et al., 2009; Lomas and Moran, 2011). Small nano- and picoplankton dominate the phytoplankton community in the oligotrophic gyres and high-nutrient, low-chlorophyll (HNLC) oceanographic regions. It has traditionally been thought that small phytoplankton represent a relatively small fraction of the downward flux of particulate organic carbon (POC) relative to larger phytoplankton, such as diatoms, which are generally thought to contribute disproportionately to POC export (e.g., Michaels and Silver, 1988). Recent studies have challenged this idea, suggesting that small phytoplankton contribute to POC export in proportion to their contribution to biomass, possibly through aggregation and incorporation into fecal pellets (Richardson and Jackson, 2007; Stukel and Landry, 2010; Lomas and Moran, 2011). A better understanding of the controls on the relative importance of small phytoplankton in POC export is needed to refine our understanding of the magnitude and mechanisms controlling the biological pump, particularly as recent climate models predict an expansion of the oligotrophic gyres where small cells dominate (Irwin et al., 2006; Polovina et al., 2008; Morán et al., 2010).

Ocean Station Papa (OSP, 50° N, 145° W), the site of one of the longest-running ocean time-series, is located in the northeast Pacific Ocean in one of three major HNLC regions. Previous attempts to resolve the apparent paradox of low phytoplankton biomass and high nitrate concentrations at OSP concluded that a bottom–up control related to iron limitation is most important for large phytoplankton (Muggli et al., 1996; Harrison, 2006; Marchetti et al., 2006), while microzooplankton grazing exerts a strong top–down control on pico- and nanoplankton (Landry et al., 1993; Harrison et al., 1999; Rivkin et al., 1999). Primary production at the stations proximal to the coast on Line P (P4 & P12) is not iron-limited and diatom blooms are typically observed in spring and late summer (Boyd and Harrison, 1999; Thibault et al., 1999). At the offshore stations (including OSP) the phytoplankton community is dominated by cells $< 5\,\mu\text{m}$ and the seasonal variability of primary production is relatively low ($\sim 25\,\text{mmol C m}^{-2}\,\text{d}^{-1}$ in winter and $\sim 67\,\text{mmol C m}^{-2}\,\text{d}^{-1}$ in summer) (Boyd and Harrison, 1999; Thibault et al., 1999; Choi et al., 2014). In contrast to the low variability in primary production, POC export recorded by moored sediment traps at OSP exhibits a stronger seasonal cycle with fluxes at 200 m depth ranging from $\sim 0.4\,\text{mmol C m}^{-2}\,\text{d}^{-1}$ in winter to $\sim 2.4\,\text{mmol C m}^{-2}\,\text{d}^{-1}$ in summer (Timothy et al., 2013). The average annual sediment trap POC flux at OSP ($1.4 \pm 1.1\,\text{mmol C m}^{-2}\,\text{d}^{-1}$) is nearly five times lower than the annual net community production (ANCP) at OSP ($6.3 \pm 1.6\,\mathrm{mmol\,C\,m^{-2}\,d^{-1}}$), suggesting that the majority of organic carbon export is due to active transport by zooplankton and/or DOC export (Timothy et al., 2013; Emerson, 2014).

This study builds upon prior investigations of phytoplankton community composition and export production along Line P by examining the distributions of organic carbon, phytoplankton indicator pigments, and ^{234}Th in three particle size-fractions. Sinking fluxes of POC and indicator pigments from the upper waters (~ 100 m) were calculated from the ^{234}Th–^{238}U disequilibrium and, during two cruises, measured at OSP using free-floating sediment traps. A comparison of indicator pigment fluxes with the respective standing stocks suggests that microplankton (20–200 µm) make up a higher percentage of POC export than biomass, whereas pico- and nano plankton (0.2–2 µm and 2–20 µm) make up a lower percentage of POC export than biomass.

2 Methods

2.1 Study location

Sample collection was conducted at five stations along Line P (P4, P12, P16, P20, and P26 (OSP)) during cruises aboard the *CCGS John P. Tully* in August 2010, February 2011, June 2011, February 2012, and June 2012 (Fig. 1, Table 1). Line P is located at the southern edge of the Alaskan Gyre, and the prevailing winds and surface currents are west-east (Bograd et al., 1999). Because precipitation and continental run-off exceed evaporation, a permanent halocline exists at ~ 100 m impeding deep winter mixing. In addition, a seasonal thermocline forms at ~ 50 m in spring and shoals to ~ 20 m in summer (Freeland et al., 1997; Thibault et al., 1999; Freeland, 2013; Timothy et al., 2013).

2.2 Net primary production by ^{14}C incubation

Rates of net primary production (NPP) were determined following the protocols outlined in Lomas et al. (2012). Samples were collected with Niskin bottles from seven depths in the euphotic zone corresponding to 1, 5, 9, 17, 33, 55, and 100 % of surface irradiance. Three “light” bottles, a single “dark” bottle, and a single initial (T) bottle were each spiked with ~ 10 µCi $NaH^{14}CO_3$. A sub-sample to confirm total added activity was removed from the T bottle at each light depth and immediately added to an equal volume of β-phenylethylamine. Bottles were incubated under simulated in situ conditions, using neutral density screening to mimic light levels at the depth of sample collection, in an on-deck incubator for ~ 24 h. After incubation, 125 mL sub-samples from each light and dark bottle were filtered through an Ahlstrom 151 (0.7 µm nominal pore size) and a Whatman Track Etch 5 µm filter and rinsed with 10 % HCl. Samples were counted on a Perkin Elmer TriCarb 2900LR ~ 48 h after the addition of 5 mL of Ultima Gold (Perkin Elmer, USA) scintillation cocktail.

2.3 Water column ^{234}Th

Total ^{234}Th (dissolved + particulate) analysis followed the procedures outlined in Bauman et al. (2013). Briefly, samples (4 L) were collected by Niskin bottle at 12 depths (surface to ~ 500 m) and spiked with ^{230}Th to monitor Th recovery. Samples were then treated with 7–8 drops of concentrated NH_4OH solution, followed by 25 µL of 0.2 M $KMnO_4$, and finally with 11.5 µL of 1.0 M $MnCl_2$ to form a MnO_2 precipitate that quantitatively scavenges Th (Benitez-Nelson et al., 2001; Buesseler et al., 2001; van der Loeff et al., 2006). After 1 h, samples were vacuum filtered onto 25 mm glass microfiber filters (GM/F, 1 µm nominal pore size) that were frozen for later analysis in the shore-based laboratory. To prepare samples for counting, filters were dried at 50 °C for ~ 24 h, mounted on acrylic planchets, and covered with aluminum foil. To quantify ^{234}Th, the beta emission of ^{234m}Pa (E_{max} = 2.19 MeV; $t_{1/2}$ = 1.2 min) was counted using a RISØ National Laboratory low-background beta detector (Roskilde, Denmark).

Each sample was counted four times over a period of approximately six half-lives, with the first count made at least 10 days after collection to allow for the decay of short-lived isotopes, and the final count used to quantify background levels. Data were fitted to the ^{234}Th decay curve to calculate the decay-corrected activity at the time of sample collection.

2.4 Water column POC, Chl *a*, and indicator pigments

Water samples for POC, Chl *a*, and phytoplankton indicator pigments were collected from the same depths in the photic zone as for NPP samples. Suspended POC was measured on 1 L seawater samples filtered onto pre-combusted Ahlstrom 151 filters and frozen at −20 °C until analysis. Samples were dried at 60 °C in a drying over, fumed in a desiccator containing concentrated hydrochloric acid for 24 h to remove inorganic carbonates, and dried again at 60 °C. Samples were then analyzed on an EA-440 Analyzer (Exeter Analytical, Inc., Chelmsford, MA) (Pike and Moran, 1997). Chl *a* samples were analyzed using the methods outlined in Lomas et al. (2012). Separate samples (∼ 0.2 L) were filtered onto Ahlstrom 151 and 5 µm Whatman Track Etch polycarbonate filters and frozen at −20 °C until analysis. Samples were then extracted in 5 mL of 90 % acetone for 24 h at −20 °C and analyzed using a calibrated TD-700 fluorometer.

Indicator pigment samples were collected on separate Ahlstrom 151 filters and stored at −80 °C until analysis by high-performance liquid chromatography (HPLC) at the Bermuda Institute of Ocean Sciences in the Bermuda Atlantic Time-series Study Laboratory (Knap et al., 1997). Fucoxanthin (FUCO), peridinin (PER), 19’-hexanoyloxyfucoxanthin (HEX), 19’-butanoyloxyfucoxanthin (BUT), alloxanthin (ALLO), total chlorophyll *b* (TChl *b*), and zeaxanthin (ZEA) were analyzed as indicator pigments based on their correspondence to particular phytoplankton taxonomic groups. Indicator proportion factors (PFs) were calculated to further analyze the size-distribution of the phytoplankton community (Hooker et al., 2005; Lomas and Moran, 2011). The sum of FUCO and PER concentrations was used to determine the microplankton proportion factor (mPF), while the sum of HEX, BUT, ALLO, and TChl *b* was used to determine the nanoplankton proportion factor (nPF), and ZEA was used to determine the picoplankton proportion factor (pPF) (Hooker et al., 2005; Lomas and Moran, 2011). Hooker et al. (2005) included TChl *b* in pPF, but because *Prochlorococcus* is not found in the study region, it was assumed in this study that any Chl *b* would be found in cells (e.g., chlorophytes and euglenophytes) in the nanoplankton size-class.

2.5 In situ pump sampling

Large-volume in situ pumps (Challenger Oceanic Systems and Services, UK and McLane Scientific, Falmouth, MA) were deployed for approximately four hours at depths of 30, 50, 100, 150, and 200 m. Each pump sampled 100–1000 L to collect size-fractionated particles, with seawater passing sequentially through 53 µm, 10 µm, and 1 µm Nitex screens. Particles were resuspended by ultrasonication in 0.7 µm prefiltered seawater and filtered onto separate pre-combusted GF/F filters for parallel analysis. Indicator pigment samples were stored at −80 °C until analysis by high-performance liquid chromatography (HPLC) at the Bermuda Institute of Ocean Sciences in the Bermuda Atlantic Time-series Study Laboratory (Knap et al., 1997). Filters for analysis of POC and ^{234}Th were frozen at −2 °C until analysis. A sub-sample (∼ 30 % by weight) was cut with acetone-cleaned stainless steel scissors from each ^{234}Th filter for POC analysis, and these sub-samples were dried and fumed with concentrated HCl as described above. POC was then measured using a CE 440 CHN Elemental Analyzer (Exeter Analytical, Inc., Chelmsford, MA). The ^{234}Th filter subsample was dried at 60 °C in a drying oven and counted on a RISØ beta detector as noted above.

2.6 Sediment trap sampling

Surface-tethered particle interceptor traps (PITS) with cylindrical tubes (KC-Denmark, Silkeborg, Denmark) were deployed for ∼ 3 days at station P26 during the June 2011 and June 2012 cruises to collect particles at the depths of 30, 50, 100, 150, and 200 m. Due to limited wire-time and other cruise constraints it was not possible to deploy sediment traps at any other stations sampled as part of this study. The trap design and sampling procedure is described in Baumann et al. (2012). Four tubes (72 mm diameter, 450 mm length) were used at each depth, and tubes were filled with non-poisoned, 0.4 µm filtered brine ($S = \sim 85$ ‰) prior to deployment. Upon recovery trap brines were combined, particles were re-suspended and filtered onto pre-combusted GF/F filters, and swimmers were removed. Filters were stored frozen and later analyzed for POC, ^{234}Th, and indicator pigments as described above.

3 Results

3.1 Hydrography and NPP

Depth sections of temperature and density anomaly (sigma-t) were generated using results from all CTD casts for a given cruise to improve horizontal data resolution (Fig. 2). The seasonal change in water temperature is largely confined to the upper ~ 100 m. Surface temperatures in August 2010 were ~ 14 °C, while during the February cruises, surface temperatures were slightly cooler offshore (~ 6 °C) than inshore (~ 8 °C). During the June cruises, inshore temperatures were warmer (~ 10–12 °C) while offshore temperatures remained relatively cool (~ 8 °C). Density anomaly did not vary greatly between cruises below ~ 100 m. During the winter, a pool of less dense water (density of 1023–1025 kg m^{-3}) was observed toward the coast (east of ~ 126° W). During the June cruises, this pool was observed extending west to ~ 130° W and during August 2010, it extended out to OSP (145° W). These data follow the expected seasonal pattern of a well-mixed water column in winter and increasing stratification moving from spring to summer.

Total NPP and > 5 µm size-fractionated NPP values were trapezoidally integrated over the euphotic zone (Table 2). A maximum total NPP of 91.9 mmol m^{-2} d^{-1} was measured at station P26 during June 2011, whereas the lowest value of 12.4 mmol m^{-2} d^{-1} was measured at station P26 during February 2012. These values agree to within a factor of two with the seasonal averages reported by Boyd and Harrison (1999). A maximum > 5 µm NPP of 39.6 $\mathrm{mmol\,m^{-2}\,d^{-1}}$ was at station P4 during June 2012 and a minimum of 2.2 $\mathrm{mmol\,m^{-2}\,d^{-1}}$ was measured at station P12 in February 2012.

3.2 Small- and large-volume POC concentrations

Suspended POC concentrations from Niskin bottle samples collected in the photic zone range from 1.1–7.1 $\mathrm{\mu mol\,L^{-1}}$. POC concentrations were generally lowest at the base of the photic zone, though decreasing concentrations with depth were not observed at all stations (Table S1). The highest suspended POC concentrations were measured at station P4 during all cruises. POC concentrations were also measured in three size-fractions of particles collected with large-volume in situ pumps (Table S2). Concentrations of each size-fraction tended to decrease with depth and were typically less than 0.5 $\mathrm{\mu mol\,L^{-1}}$ at all depths. One exception was at station P26 during February 2011 when POC concentrations at 30 m were between 1.8 and 2.9 $\mathrm{\mu mol\,L^{-1}}$ for all size-fractions.

The concentrations of POC collected using small-volume and large-volume methods often do not agree for samples collected at the same location and depth (Gardner, 1977; Moran et al., 1999; Liu et al., 2005, 2009). As reported in these previous studies, POC concentrations measured by large-volume in situ pumps (summed for all size-fractions) are significantly (ANOVA, $p < 0.05$) less than small-volume POC measurements from the same station and similar depth (Fig. 3a). Explanations put forth to account for this discrepancy include DOC adsorption to filters, pressure effects on particle retention in pump samples, the collection of zooplankton by Niskin bottles but not pumps, and particle washout from pump filters (Moran et al., 1999; Liu et al., 2005, 2009). In this study, the smallest pump size-fraction was collected using a 1 µm Nitex screen, not a GF/F, resulting in the pumps missing the portion of the POC on particles between 0.7 and 1 µm, which may further contribute to the difference observed between the two methods. Lomas and Moran (2011) reported that sonication of in situ pump samples to resuspend particles from the Nitex screens had no significant effect on measured POC concentrations.

3.3 Particulate ^{234}Th and POC/^{234}Th ratios

Size-fractionated particulate ^{234}Th activities in samples collected by in situ pump generally decrease with depth, and are typically less than 0.1 dpm L^{-1} (Table S2). As with in situ pump POC concentrations, station P26 during February 2011 is an exception, with values exceeding 0.1 dpm L^{-1} for all size fractions at 30 m and throughout most of the water column for the 1–10 µm fraction. Size-fractionated POC/^{234}Th ratios (Fig. 4, Table S2) are less than ~ 6 µmol dpm^{-1} for all size-classes at most stations, with higher values measured at stations P4 and P12 in February 2012 and P4 in June 2012. POC/^{234}Th ratios tend to decrease or remain constant with depth, with one exception at station P12 during February 2012 where the maximum POC/^{234}Th was at 100 m for all size fractions. Also, the POC/^{234}Th ratio does not vary greatly between size-fractions (Fig. 4) as was observed in Speicher et al. (2006) and Brew et al. (2009).

The accuracy of ^{234}Th as a tracer of POC export depends on the assumption that ^{234}Th and POC are sinking on the same particles, and therefore sinking at the same rate (Moran et al., 2003; Smith et al., 2006; Speicher et al., 2006; Burd et al., 2007; Brew et al., 2009). A high degree of correlation between the size-fractionated distributions of ^{234}Th and POC (Fig. 4) along Line P provides evidence in support of this assumption. All correlations were statistically significant ($p < 0.05$) and imply a strong coupling between particulate ^{234}Th and POC for all cruises. In addition, the clustering of data for the different size-fractions of particles (Fig. 4) indicates that in February 2012 the 10–53 µm size class contained the highest percentage of POC and particulate ^{234}Th, while the > 53 µm size class contained the lowest percentage. In June 2012, the 1–10 µm size class had the lowest percentage of POC and particulate ^{234}Th while both the 10–53 µm and the > 53 µm fractions contained higher percentages (Fig. 4).

3.4 Small-volume Chl *a* and indicator pigments

Concentrations of total Chl *a* and > 5 µm Chl *a* measured by fluorometer (Table S1) were trapezoidally integrated over the photic zone to determine respective standing stocks. During August 2010, the > 5 µm fraction accounted for > 30 % of the Chl *a* at all stations, with a maximum of 50 % at station P26. During the other four cruises, the > 5 µm size-fraction generally accounted for < 30 % of the total Chl *a*, except at station P26 in February 2012 and station P4 in June 2012. Previous studies have reported that larger cells are more abundant at stations closer to the coast (Boyd and Harrison, 1999), though this was not always apparent. The highest > 5 µm percentage of Chl *a* was measured at station P26 during August 201, June 2011, and February 2012. Phytoplankton indicator pigments and Chl *a* concentrations in samples from the euphotic zone samples were also measured by HPLC (Table S1). HPLC and fluorescence Chl *a* concentrations generally agreed to within a factor of two, and the correlation between the two measurements was statistically significant ($p < 0.05$) (Fig. S1). The correlation between the sum of the indicator pigment concentrations and the Chl *a* concentration was statistically significant ($p < 0.05$) and roughly 1 : 1, suggesting that the indicator pigments examined in this analysis accounted for most of the phytoplankton biomass (Fig. S2). Furthermore, the correlation between the > 5 µm fraction of Chl *a* and mPF is statistically significant ($p < 0.05$), suggesting that this PF is a reasonable representation of that size-fraction of the phytoplankton community. Profiles of indicator pigment concentrations were trapezoidally integrated over the photic zone to quantify standing stocks (Table 3). FUCO was the most abundant microplankton pigment, and HEX was the most abundant nanoplankton pigment at most stations. Indicator pigment PFs (Fig. 5, Table S3) reveal that the phytoplankton community was typically dominated by nanoplankton, although at P4, and to a lesser extent at P20 in June 2012, microplankton pigments made up the bulk of the sample (~ 86 % and ~ 52 % respectively).

3.5 Large-volume size-fractionated Chl *a* and indicator pigments

Size-fractionated Chl *a* and indicator pigment concentrations were also measured by in situ pump (Table S4). Chl *a* was once again strongly correlated in a roughly 1 : 1 ratio with the sum of the indicator pigments ($p < 0.05$) (Fig. S3). The highest Chl *a* concentrations were measured in the 10–53 µm fraction during all cruises. In February 2012, the > 53 µm fraction generally had the lowest concentrations, while in June 2012 and June 2011 the lowest concentrations were generally in the 1–10 µm fraction.

Ideally, small-volume and large-volume concentrations of Chl *a* and indicator pigments should agree for samples collected at the same station and depth, but this was not observed in this study (Fig. 3). Although differences between small- and large-volume measurements of POC have been reported (Gardner, 1977; Moran et al., 1999; Liu et al., 2005, 2009), few studies have compared Niskin bottle and in situ pump measurements of indicator pigments (Lomas and Moran, 2011). Relative to bottle samples, the pump samples indicate higher concentrations of microplankton pigments FUCO and PER and lower concentrations of ZEA and TChl *b*, which are pigments associated with pico- and nanoplankton (Fig. 3b–d). Large-volume pump and small-volume bottle measurements of the nanoplankton indicator pigments HEX, BUT, and ALLO generally agree within a factor of two (Fig. 3b–d). Given the small size of ZEA-containing *Synechococcus* and TChl *b*-containing chlorophytes and prasinophytes, it is likely that many of these cells pass through the 1 µm Nitex screen which would lead to undersampling by the pumps (Liu et al., 2005). Bottles may undersample large, rare cells because the small volume might not be a statistically representative sample (Lomas and Moran, 2011). Furthermore, larger cells may settle below the spigot of the Niskin bottles, leading to a further bias against the collection of large cells (Gardner, 1977; Gundersen et al., 2001). Pumps sample higher concentrations of Chl *a* than bottles (Fig. 3a) at stations with high concentrations of Chl *a*, but when Chl *a* concentrations are low ($< 200\,\mathrm{ng\,L^{-1}}$), the pumps tend to undersample relative to the bottles.

Given these sampling differences, it is important to note that although the total concentrations (summed for all size-fractions) measured by the in situ pumps may be inaccurate, it is still possible that the $> 53\,\mu m$ fraction accurately represents the composition of sinking particles. The disruption of loosely-bound aggregates during collection by the pumps could cause an error in the $> 53\,\mu m$ fraction, but this is considered unlikely due to the presence of nanoplankton (and in some cases picoplankton) pigments in this fraction. Furthermore, a recent study in the Sargasso Sea employed a similar methodology and also found picoplankton pigments in three particle size-classes, each $> 10\,\mu m$ (Lomas and Moran, 2011).

Indicator pigment PFs calculated for the size-fractionated particles (Table S3) and plotted against depth (Figs. 6–8) reveal that while the overall indicator pigment concentrations vary with depth and across size-fractions, the PFs do not exhibit a systematic pattern of variation across size classes, depths, or seasons. The picoplankton pigment ZEA typically represents $< 10\,\%$ of the total indicator pigments for all size classes. Microplankton pigments dominated samples at station P4 in February 2012 and June 2012, with mPFs typically exceeding 0.5 and 0.8, respectively, for each cruise. In addition, mPFs were high at station P26 during these times, with values generally exceeding 0.5 (Figs. 7 and 8). Nanoplankton pigments dominated at station P12 in February 2012 cruise with nPFs exceeding 0.5 for most samples. As with the small volume samples, FUCO was usually the most abundant microplankton pigment while HEX was usually the most abundant nanoplankton pigment (Table S4).

3.6 Total ^{234}Th, ^{234}Th/^{238}U activity ratios, and ^{234}Th fluxes

Total (dissolved + particulate) ^{234}Th activities, ^{238}U activities, and ^{234}Th/^{238}U activity ratios are listed in Table S5. Depth sections of these ^{234}Th/^{238}U activity ratios (Fig. 2d) indicate that areas of low ^{234}Th/^{238}U are prevalent in spring and summer and corresponding to periods known to have high particle export in this region (Wong et al., 1999; Timothy et al., 2013). ^{234}Th fluxes (P_{Th}) were calculated using these ^{234}Th/^{238}U results and a 2-D steady-state model of the radiochemical balance for ^{234}Th in the upper ocean,

$$\frac{\partial A_{\mathrm{Th}}}{\partial t} = A_{\mathrm{U}}\lambda_{\mathrm{Th}} - A_{\mathrm{Th}}\lambda_{\mathrm{Th}} - P_{\mathrm{Th}} + K_h\frac{\partial^2 A_{\mathrm{Th}}}{\partial^2 x} + U_h\frac{\partial A_{\mathrm{Th}}}{\partial x} \tag{1}$$

where A_{U} is the activity of ^{238}U, λ_{Th} is the ^{234}Th decay constant, A_{Th} is the activity of ^{234}Th, P_{Th} is the vertical flux of ^{234}Th on sinking particles, K_h is the eddy diffusion coefficient, and U_h is the current velocity (Coale and Bruland, 1985; Charette et al., 1999). Assuming a steady-state ($\partial A_{\mathrm{Th}}/\partial t = 0$) over several weeks to months, and that the diffusive flux of ^{234}Th is small relative to advection and can therefore be ignored, the vertical flux of ^{234}Th is defined by,

$$P_{\mathrm{Th}} = \int_0^z \left[\lambda_{\mathrm{Th}}(A_U - A_{\mathrm{Th}}) + U_h\frac{\partial A_{\mathrm{Th}}}{\partial x}\right] \mathrm{d}z \tag{2}$$

where z is the depth of the water column over which the flux is measured. In this study, the gradient of thorium ($\partial A_{\mathrm{Th}}/\partial x$) was only measured in the east-west direction (along Line P). Therefore, x is the east-west distance across which the gradient will be measured and U_h is the east-west current velocity. Given that the currents in the region generally flow west-east, and with no data at stations north and south of Line P, the north-south transport of ^{234}Th by advection had to be assumed to be negligible. At stations P12, P16, and P20, the ^{234}Th gradient was measured between the adjacent stations. For stations P4 and P26 (at either end of Line P), the gradient of ^{234}Th was determined from the adjacent station assuming a linear change extended beyond the measured transect.

^{234}Th fluxes (P_{Th}) calculated using the 2-D model are within 5 % of fluxes determined using a steady-state 1-D model that ignores advection (Fig. S4). This indicates that, under these assumptions, the vertical flux of ^{234}Th on sinking particles is the dominant transport term. Consistent with previous studies, ^{234}Th fluxes at all stations were higher during the August and June cruises than during the February cruises (Fig. 9a) (Charette et al., 1999). Also, ^{234}Th fluxes did not exhibit a consistent trend along Line P.

3.7 ^{234}Th-derived POC fluxes

The POC/^{234}Th ratio in the $>53\,\mu$m size-class and P_{Th} for a given depth horizon were used to calculate POC fluxes (P_{POC}) (Fig. 9). In most cases, P_{POC} decreases with depth, although in some cases, the maximum P_{POC} in a given profile occurs at 50 or 100 m. P_{POC} fluxes at 100 m range from 0.65–7.95 mmol m^{-2} d^{-1}; they are generally higher in summer than winter, and highest at station P4, consistent with previous studies at Line P (Charette et al., 1999; Wong et al., 1999; Timothy et al., 2013).

The ratio of P_{POC} flux to NPP, referred to as the ThE-ratio, is an estimate of efficiency of the biological pump (Buesseler, 1998). ThE-ratios determined using P_{POC} fluxes at the base of the photic zone (Table 2, Fig. 10) are similar to those reported by Charette et al. (1999), and are also in line with an annual average *e* ratio determined using average sediment trap POC fluxes (Wong et al., 1999) and annual average NPP (Harrison, 2002) (Fig. 10).

3.8 Sediment trap ^{234}Th and POC fluxes

The particle fluxes of both ^{234}Th and POC fluxes determined by the PITS traps (F_{Th} and F_{POC} respectively) generally decreasee with depth (Table 4). F_{Th} was higher in June 2012 than in June 2011, though there was no clear difference between the two cruises for F_{POC}. A comparison of the F_{Th} with the P_{Th} from corresponding stations and depths indicates that the F_{Th} is consistently higher than the P_{Th}, though usually not by more than a factor of two. F_{POC} is also consistently higher than P_{POC}, though again not by more than a factor of two (Fig. 11a). The POC/^{234}Th ratios of particles caught in sediment traps (Table 9) tend to be slightly higher (generally within a factor of 2) than the ratio of particles sampled by pumps at the corresponding station and depth.

3.9 ^{234}Th-derived and sediment trap pigment fluxes

Sinking fluxes of Chl *a* (P_{Chla}) and indicator pigments (P_{Pigment}) were calculated from P_{Th} and the Pigment/^{234}Th ratio measured on > 53 µm particles. Chl *a* and indicator pigment fluxes (Table 3, Fig. 11a–c) are generally highest at station P4 and decrease moving offshore. The highest indicator pigment fluxes were typically observed for microplankton pigments (FUCO and PER) whereas the lowest were observed for the picoplankton pigment ZEA (Table 3, Fig. 12a–c).

Sediment trap pigment fluxes (F_{Pigment}) were typically lower than P_{Pigment} (Table 3, Fig. 11b). The maximum sediment trap fluxes of Chl *a* and most indicator pigments were determined at 50 m in June 2011 and at 30 m in June 2012 (Table 3). For both deployments the deepest fluxes were generally the lowest, presumably due to the progressive degradation of sinking phytoplankton and resulting loss of pigments. Chl *a* and indicator pigment fluxes were generally higher in June 2011 than in June 2012, which is the opposite of the trend observed for F_{Th}.

Pigment PFs determined for material captured by the PITS traps do not vary greatly with depth, suggesting that the quality of material sinking to depth is similar to that in the surface water, despite the general decrease of material (Figs. 6 and 8). Microplankton PFs are higher for trap samples than for bottle samples but not as high as for pump samples, while nPFs and pPFs are higher for trap samples than for pump samples but lower than for bottle samples.

4 Discussion

The results presented in this study build on previous investigations of export production in the northeast Pacific by providing estimates of the relative contributions of different phytoplankton size-classes to particle export. A comparison of indicator pigment standing stocks and P_{Pigment} fluxes suggests that while nanoplankton represented the bulk of phytoplankton biomass (68 ± 24 % of pigment standing stock, averaged for all stations and cruises), microplankton dominated the flux of pigmented material (69 ± 19 % on average) (Table 3, Fig. 12). Sediment trap pigment fluxes indicate a lower, but still substantial, relative contribution of microplankton to export, with microplankton pigments making up 47 % and 33 % of the total sediment trap indicator pigment flux in June 2011 and June 2012 respectively, as compared to 81 % and 85 % of total P_{Pigment} fluxes. Though nano- and picoplankton did not form the majority of the algal aggregate flux, their 29 ± 19 % contribution is significant and similar to contributions reported by Lomas and Moran (2011) for cyanobacteria and nano-eukaryotes in the Sargasso Sea.

Indicator pigment loss rates determined from both P_{Pigment} fluxes and sediment trap pigment fluxes imply that microplankton are exported more efficiently than nano- or picoplankton (Table 3, Fig. 12d–f). Loss rates of pigments, estimated as the ratio of P_{Pigment} fluxes to pigment standing stock, averaged (for all cruises) 8 ± 12 % for microplankton pigments, 1 ± 2 % for nanoplankton pigments and 0.6 ± 1 % for picoplankton pigments. These results suggest that export of large cells by direct sinking of algal aggregates is more efficient than the export of small cells by the same pathway. Sediment trap loss rates for microplankton were also higher than those for nano- and picoplankton, further indicating preferential export of microplankton. Even though differences between bottle and pump samples may exaggerate the extent to which large cells dominate export, sediment trap loss rates support and confirm the preferential export of large cells by algal aggregation.

In contrast to the trends observed for pigment fluxes and loss rates, the low variability of pump indicator pigment PFs with depth (Figs. 6–8) does not appear to indicate preferential export of microplankton. Furthermore, the presence of nano- and picoplankton pigments in the > 53 µm size-fraction and in samples below the mixed layer suggests that nano- and picoplankton are incorporated into aggregates and that some of these aggregates are exported from the surface ocean. If large cells were being preferentially exported, microplankton pigments would be expected to make up a larger percentage of total pigments in samples below the mixed layer than in samples from the mixed layer, but this is not observed in the results of this study. It is possible that some of this discrepancy can be attributed to differences between bottle and pump samples. Because cells < 1 µm in size can pass through the 1 µm Nitex screens used in the pumps, the sum of the pump size-fractions does not accurately reflect the community composition in the euphotic zone, and may miss a change in indicator pigment PFs with depth. In addition, the under-sampling of large cells by Niskin bottles may lead to an underestimate of microplankton standing stocks, and thus and overestimate of microplankton loss rates.

These pigment fluxes are likely lower estimates of the total contribution of each phytoplankton group to particle export. The use of indicator pigments as tracers of phytoplankton export only accounts for the direct sinking of healthy, ungrazed cells, because grazing degrades the indicator pigments to an analytically undetectable form (Head and Harris, 1992; Strom et al., 1998; Thibault et al., 1999). Indirect export (via grazing) is thought to be an important pathway for picoplankton export in the HNLC Equatorial Pacific (Richardson et al., 2004; Stukel and Landry, 2010). Given that grazing has been shown to control the biomass of small phytoplankton in the northeast Pacific (Landry et al., 1993; Harrison et al., 1999; Rivkin et al., 1999), indirect export may also be a significant pathway for small cell export in this region. Because this pathway is not accounted for by the methodology employed in this study, the results presented here may underestimate the export of small phytoplankton, which may be less likely to sink directly.

Although grazing and fecal pellet export were not directly measured in this study, a comparison of sediment trap and pump measurements of Chl *a*, indicator pigments, and POC, suggests that zooplankton fecal pellets may be an important component of POC export at OSP, at least in spring (Fig. 11). While F_{POC} fluxes are higher than the corresponding P_{POC} fluxes, F_{Pigment} fluxes are lower than P_{Pigment} fluxes, indicating that the material captured by the sediment traps is enriched in carbon and depleted in Chl *a* and indicator pigments relative to that sampled by the pumps. Because the trap brine was not poisoned, zooplankton grazing and cell degradation in the trap tube may also have contributed to some loss of pigments over the ~ 3 day deployment of the PITS traps. However, the collection of carbon-rich and pigment-depleted fecal pellets by the traps but not by the pumps, which do not quantitatively sample fecal pellets (Lomas and Moran, 2011), could also explain these observations. This latter explanation is consistent with the results presented in Thibault et al. (1999), which indicate that fecal pellet export is 3 to 6 times greater than algal aggregate export at Line P.

5 Conclusions

New estimates of phytoplankton indicator pigment loss rates calculated from both ^{234}Th-derived and sediment trap pigment fluxes suggest that large cells are preferentially exported at Line P. Specifically, microplankton pigments on average made up 69 ± 19 % of the total pigment flux, but only 32 ± 24 % of pigment standing stock, whereas nano- and picoplankton pigments on average formed 31 ± 19 % of pigment flux in spite of representing 68 ± 24 % of the standing stock. These results are consistent with traditional food web models (Michaels and Silver, 1988; Legendre and Le Fèvre, 1995) that suggest nano- and picoplankton are underrepresented in particle flux relative to their contribution to phytoplankton biomass; they also lend support to the conclusions of Choi et al. (2014). However, the methods employed in this study do not quantitatively account for export via zooplankton fecal pellets, which could be significant for small phytoplankton as they are controlled by grazing in this region (Landry et al., 1993; Harrison et al., 1999; Rivkin et al., 1999; Thibault et al., 1999). Furthermore, the determination of pigment loss rates also required a comparison between small- and large-volume samples, and the inherent differences of these sampling techniques likely led to an overestimation of the microplankton contribution to algal aggregate export. Therefore, it is possible that all sizes-classes of phytoplankton contribute to POC export in approximate proportion to their contribution to NPP as predicted by Richardson and Jackson (2007).

This study, conducted in a subarctic HNLC region, contributes to the ongoing discussion of small cell export that has largely focused on tropical and subtropical regions

(Richardson et al., 2004, 2006; Richardson and Jackson, 2007; Stukel and Landry, 2010; Lomas and Moran, 2011). In particular, these results suggest that nano- and picoplankton may contribute significantly to POC export in this subarctic HNLC region, even if they are not as efficiently exported as larger microplankton. If large phytoplankton drive more efficient POC export in the northeast Pacific as suggested by this study, it could have important implications for understanding the biological pump. It has been proposed that decreasing winter mixed layer depths (Freeland et al., 1997; Freeland, 2013) and variations of macronutrient concentrations linked to shifts in climate regime (Pena and Varela, 2007) in the northeast Pacific could lead to shifts in the phytoplankton community composition. This study suggests that such changes in phytoplankton community composition could significantly affect the efficiency of the biological pump, and in turn, the cycling of carbon. While the results indicate that shifts in community composition favoring larger phytoplankton could lead to more efficient particle export, they do not indicate that shifts favoring smaller phytoplankton would lead to a shutdown of POC export as suggested by some previous studies (e.g., Michaels and Silver, 1988), but merely that the export of POC could be less efficient.

The Supplement related to this article is available online at doi:10.5194/bgd-11-12631-2014-supplement.

Acknowledgements. We thank the captain and crew of the *CCGS John P. Tully*, Marie Robert and the Line P Program collaborators, Doug Bell for at-sea sampling and laboratory assistance, and Matthew Baumann for his laboratory assistance. This research was supported by the National Science

Foundation grants OCE 0926311 to SBM, OCE 0927559 to MWL, and OCE 0926348 to GMS.

References

Baumann, M. S., Moran, S. B., Lomas, M. W., Kelly, R. P., and Bell, D. W.: Seasonal decoupling of particulate organic carbon export and net primary production in relation to sea-ice at the shelf break of the eastern Bering Sea: implications for off-shelf carbon export, J. Geophys. Res.-Oceans, 118, 5504–5522, doi:10.1002/jgrc.20366, 2013.

Benitez-Nelson, C. R., Buesseler, K. O., Van der Loeff, M. R., Andrews, J., Ball, L., Crossin, G., and Charette, M. A.: Testing a new small-volume technique for determining ^{234}Th in seawater, J. Radioanal. Nucl. Ch., 248, 795–799, 2001.

Bograd, S. J., Thomson, R. E., Rabinovich, A. B., and LeBlond, P. H.: Near-surface circulation of the northeast Pacific Ocean derived from WOCE-SVP satellite-tracked drifters, Deep-Sea Res. Pt. II, 46, 2371–2403, doi:10.1016/S0967-0645(99)00068-5, 1999.

Boyd, P. and Harrison, P. J.: Phytoplankton dynamics in the NE subarctic Pacific, Deep-Sea Res. Pt. II, 46, 2405–2432, doi:10.1016/S0967-0645(99)00069-7, 1999.

Boyd, P. W. and Newton, P. P.: Does planktonic community structure determine downward particulate organic carbon flux in different oceanic provinces?, Deep-Sea Res. Pt. I, 46, 63–91, doi:10.1016/S0967-0637(98)00066-1, 1999.

Brew, H. S., Moran, S. B., Lomas, M. W., and Burd, A. B.: Plankton community composition, organic carbon and thorium-234 particle size distributions, and particle export in the Sargasso Sea, J. Mar. Res., 67, 845–868, doi:10.1357/002224009792006124, 2009.

Buesseler, K. O.: The decoupling of production and particulate export in the surface ocean, Global Biogeochem. Cy., 12, 297–310, doi:10.1029/97GB03366, 1998.

Buesseler, K. O., Benitez-Nelson, C., Rutgers van der Loeff, M., Andrews, J., Ball, L., Crossin, G., and Charette, M. A.: An intercomparison of small-and large-volume techniques for thorium-234 in seawater, Mar. Chem., 74, 15–28, 2001.

Burd, A. B., Jackson, G. A., and Moran, S. B.: The role of the particle size spectrum in estimating POC fluxes from disequilibrium, Deep-Sea Res. Pt. I, 54, 897–918, 2007.

Charette, M. A., Moran, S. B., and Bishop, J. K. B.: ^{234}Th as a tracer of particulate organic carbon export in the subarctic northeast Pacific Ocean, Deep-Sea Res. Pt. II, 46, 2833–2861, doi:10.1016/S0967-0645(99)00085-5, 1999.

Choi, H. Y., Stewart, G. M., Lomas, M. W., Kelly, R. P., and Moran, S. B.: Linking the distribution of ^{210}Po and ^{210}Pb with plankton community along Line P, Northeast Subarctic Pacific, J. Environ. Radioactiv., doi:10.1016/j.jenvrad.2014.02.009, in press, 2014.

Coale, K. H. and Bruland, K. W.: ^{234}Th : ^{238}U disequilibria within the California Current, Limnol. Oceanogr., 30, 22–33, 1985.

Emerson, S.: Annual net community production and the biological carbon flux in the ocean, Global Biogeochem. Cy., 28, 14–28, doi:10.1002/2013GB004680, 2014.

Freeland, H. J.: Evidence of change in the winter mixed layer in the Northeast Pacific Ocean: a problem revisited, Atmos. Ocean, 51, 126–133, 2013.

Freeland, H., Denman, K., Wong, C. S., Whitney, F., and Jacques, R.: Evidence of change in the winter mixed layer in the Northeast Pacific Ocean, Deep-Sea Res. Pt. I, 44, 2117–2129, doi:10.1016/S0967-0637(97)00083-6, 1997.

Gardner, W. D.: Incomplete extraction of rapidly settling particles from water samplers, Limnol. Oceanogr., 22, 764–768, 1977.

Gundersen, K., Orcutt, K. M., Purdie, D. A., Michaels, A. F., and Knap, A. H.: Particulate organic carbon mass distribution at the Bermuda Atlantic Time-series Study (BATS) site, Deep-Sea Res. Pt. II, 48, 1697–1718, 2001.

Harrison, P. J.: SERIES (subarctic ecosystem response to iron enrichment study): A Canadian–Japanese contribution to our understanding of the iron–ocean–climate connection, Deep-Sea Res. Pt. II, 53, 2006–2011, doi:10.1016/j.dsr2.2006.08.001, 2006.

Harrison, P. J., Boyda, P. W., Varela, D. E., Takeda, S., Shiomoto, A., and Odate, T.: Comparison of factors controlling phytoplankton productivity in the NE and NW subarctic Pacific gyres, Prog. Oceanogr., 43, 205–234, doi:10.1016/S0079-6611(99)00015-4, 1999.

Head, E. J. H. and Harris, L. R.: Chlorophyll and carotenoid transformation and destruction by Calanus spp. grazing on diatoms, Mar. Ecol.-Prog. Ser., 86, 229–229, 1992.

Hooker, S. B., Van Heukelem, L., Thomas, C. S., Claustre, H., Ras, J., Barlow, R., Sessions, H., Schlüter, L., Perl, J., and Trees, C.: Second SeaWiFS HPLC Analysis Round-robin Experiment (SeaHARRE-2), National Aeronautics and Space Administration, Goddard Space Flight Center, 2005.

Irwin, A. J., Finkel, Z. V., Schofield, O. M. E., and Falkowski, P. G.: Scaling-up from nutrient physiology to the size-structure of phytoplankton communities, J. Plankton Res., 28, 459–471, doi:10.1093/plankt/fbi148, 2006.

Knap, A. H., Michaels, A. F., Steinberg, D. K., Bahr, F., Bates, N. R., Bell, S., Countway, P., Close, A. R., Doyle, A. P., and Dow, R. L.: BATS Methods manual, version 4, 1997.

Landry, M. R., Monger, B. C., and Selph, K. E.: Time-dependency of microzooplankton grazing and phytoplankton growth in the subarctic Pacific, Prog. Oceanogr., 32, 205–222, doi:10.1016/0079-6611(93)90014-5, 1993.

Legendre, L. and Le Fèvre, J.: Microbial food webs and the export of biogenic carbon in oceans, Aquat. Microb. Ecol., 9, 69–77, 1995.

Liu, Z., Stewart, G., Kirk Cochran, J., Lee, C., Armstrong, R. A., Hirschberg, D. J., Gasser, B., and Miquel, J.-C.: Why do POC concentrations measured using Niskin bottle collections sometimes differ from those using in-situ pumps?, Deep-Sea Res. Pt. I, 52, 1324–1344, doi:10.1016/j.dsr.2005.02.005, 2005.

Liu, Z., Cochran, J. K., Lee, C., Gasser, B., Miquel, J. C., and Wakeham, S. G.: Further investigations on why POC concentrations differ in samples collected by Niskin bottle and in situ pump, Deep-Sea Res. Pt. II, 56, 1558–1567, doi:10.1016/j.dsr2.2008.12.019, 2009.

Lomas, M. W. and Moran, S. B.: Evidence for aggregation and export of cyanobacteria and nano-eukaryotes from the Sargasso Sea euphotic zone, Biogeosciences, 8, 203–216, doi:10.5194/bg-8-203-2011, 2011.

Lomas, M. W., Moran, S. B., Casey, J. R., Bell, D. W., Tiahlo, M., Whitefield, J., Kelly, R. P., Mathis, J. T., and Cokelet, E. D.: Spatial and seasonal variability of primary production on the Eastern Bering Sea shelf, Deep-Sea Res. Pt. II, 65, 126–140, doi:10.1016/j.dsr2.2012.02.010, 2012.

Marchetti, A., Sherry, N. D., Kiyosawa, H., Tsuda, A., and Harrison, P. J.: Phytoplankton processes during a mesoscale iron enrichment in the NE subarctic Pacific: Part I – biomass and assemblage, Deep-Sea Res. Pt. II, 53, 2095–2113, 2006.

Michaels, A. F. and Silver, M. W.: Primary production, sinking fluxes and the microbial food web, Deep-Sea Res. Pt. I, 35, 473–490, doi:10.1016/0198-0149(88)90126-4, 1988.

Moran, S. B., Charette, M. A., Pike, S. M., and Wicklund, C. A.: Differences in seawater particulate organic carbon concentration in samples collected using small-and large-volume methods: the importance of DOC adsorption to the filter blank, Mar. Chem., 67, 33–42, 1999.

Moran, S. B., Weinstein, S. E., Edmonds, H. N., Smith, J. N., Kelly, R. P., Pilson, M. E. Q., and Harrison, W. G.: Does ^{234}Th/^{238}U disequilibrium provide an accurate record of the export flux of particulate organic carbon from the upper ocean?, Limnol. Oceanogr., 48, 1018–1029, 2003.

Morán, X. A. G., López-Urrutia, Á., Calvo-Díaz, A., and Li, W. K.: Increasing importance of small phytoplankton in a warmer ocean, Glob. Change Biol., 16, 1137–1144, 2010.

Muggli, D. L., Lecourt, M., and Harrison, P. J.: Effects of iron and nitrogen source on the sinking rate, physiology and metal composition of an oceanic diatom from the subarctic Pacific, Mar. Ecol.-Prog. Ser., 132, 215–227, 1996.

Pena, M. A. and Varela, D. E.: Seasonal and interannual variability in phytoplankton and nutrient dynamics along Line P in the NE subarctic Pacific, Prog. Oceanogr., 75, 200–222, 2007.

Pike, S. M. and Moran, S. B.: Use of Poretics® 0.7 µm pore size glass fiber filters for determination of particulate organic carbon and nitrogen in seawater and freshwater, Mar. Chem., 57, 355–360, 1997.

Polovina, J. J., Howell, E. A., and Abecassis, M.: Ocean's least productive waters are expanding, Geophys. Res. Lett., 35, L03618, doi:10.1029/2007GL031745, 2008.

Richardson, T. L. and Jackson, G. A.: Small phytoplankton and carbon export from the surface ocean, Science, 315, 838–840, 2007.

Richardson, T. L., Jackson, G. A., Ducklow, H. W., and Roman, M. R.: Carbon fluxes through food webs of the eastern equatorial Pacific: an inverse approach, Deep-Sea Res. Pt. I, 51, 1245–1274, doi:10.1016/j.dsr.2004.05.005, 2004.

Richardson, T. L., Jackson, G. A., Ducklow, H. W., and Roman, M. R.: Spatial and seasonal patterns of carbon cycling through planktonic food webs of the Arabian Sea determined by inverse analysis, Deep-Sea Res. Pt. II, 53, 555–575, doi:10.1016/j.dsr2.2006.01.015, 2006.

Rivkin, R. B., Putland, J. N., Robin Anderson, M., and Deibel, D.: Microzooplankton bacterivory and herbivory in the NE subarctic Pacific, Deep-Sea Res. Pt. II, 46, 2579–2618, 1999.

Speicher, E. A., Moran, S. B., Burd, A. B., Delfanti, R., Kaberi, H., Kelly, R. P., Papucci, C., Smith, J. N., Stavrakakis, S., and Torricelli, L.: Particulate organic carbon export fluxes and size-fractionated POC/^{234}Th ratios in the Ligurian, Tyrrhenian and Aegean Seas, Deep-Sea Res. Pt. I, 53, 1810–1830, 2006.

Strom, S., Morello, T., and Bright, K.: Protozoan size influences algal pigment degradation during grazing, Mar. Ecol.-Prog. Ser., 164, 189–197, doi:10.3354/meps164189, 1998.

Stukel, M. R. and Landry, M. R.: Contribution of picophytoplankton to carbon export in the equatorial Pacific: a reassessment of food web flux inferences from inverse models, Limnol. Oceanogr., 55, 2669–2685, 2010.

Thibault, D., Roy, S., Wong, C. S., and Bishop, J. K.: The downward flux of biogenic material in the NE subarctic Pacific: importance of algal sinking and mesozooplankton herbivory, Deep-Sea Res. Pt. II, 46, 2669–2697, 1999.

Timothy, D. A., Wong, C. S., Barwell-Clarke, J. E., Page, J. S., White, L. A., and Macdonald, R. W.: Climatology of sediment flux and composition in the subarctic Northeast Pacific Ocean with biogeochemical implications, Prog. Oceanogr., 116, 95–129, 2013.

Van der Loeff, M. R., Sarin, M. M., Baskaran, M., Benitez-Nelson, C., Buesseler, K. O., Charette, M., Dai, M., Gustafsson, Ö., Masque, P., and Morris, P. J.: A review of present techniques and methodological advances in analyzing ^{234}Th in aquatic systems, Mar. Chem., 100, 190–212, 2006.

Wong, C. S., Whitney, F. A., Crawford, D. W., Iseki, K., Matear, R. J., Johnson, W. K., Page, J. S., and Timothy, D.: Seasonal and interannual variability in particle fluxes of carbon, nitrogen and silicon from time series of sediment traps at Ocean Station P, 1982–1993: relationship to changes in subarctic primary productivity, Deep-Sea Res. Pt. II, 46, 2735–2760, 1999.

Table 1. Cruise dates and sample collection along Line P.

Cruise Dates	P4	P12	P16	P20	P26
2010-14 Aug 2010 (19–31 Aug 2010)	Total Th	Total Th WC Pig	Total Th WC Pig	Total Th WC Pig	Total Th
2011-01 Feb 2011 (9–15 Feb 2011)		Total Th WC Pig	Total Th WC Pig	Total Th WC Pig	Total Th
2011-26 Jun 2011 (4–16 Jun 2011)	Total Th WC Pig	Total Th WC Pig	Total Th WC Pig	Total Th WC Pig	Total Th Part. Th WC Pig Part. Pig Traps
2012-01 Feb 2012 (7–19 Feb 2012)	Total Th Part. Th WC Pig Part. Pig	Total Th Part. Th WC Pig Part. Pig	Total Th	Total Th	Total Th Part. Th WC Pig Part. Pig
2012-12 Jun 2012 (23 May–7 Jun 2012)	Total Th Part. Th WC Pig Part. Pig	Total Th Part. Th WC Pig Part. Pig	Total Th Part. Th WC Pig Part. Pig	Total Th Part. Th Part. Pig	Total Th Part. Th Part. Pig Traps

Table 2. Total NPP and > 5 µm size-fractionated NPP determined from simulated in situ incubations. P_{POC} and $\mathrm{Trap}_{\mathrm{POC}}$ determined at the base of the photic zone and the corresponding ThE-ratios and trap *e* ratios.

Cruise	Station	Integration Depth(m)	Total NPP (mmol m^{-2} d^{-1})	> 5 µm NPP (mmol m^{-2} d^{-1})	P_{POC} (mmol m^{-2} d^{-1})	$\mathrm{Trap}_{\mathrm{POC}}$ (mmol m^{-2} d^{-1})	ThE -ratio	Trap *e* ratio
Feb 2011	P20	77	36.64	3.26				
Jun 2011	P26-D	83	105.14	13.67	2.94	5.91	0.03	0.06
	P26-R	85	78.75	12.98	2.75	5.91	0.03	0.08
Feb 2012	P4	50	27.91	3.58	7.29		0.26	
	P12	95	34.56	4.58	4.65		0.13	
	P26	75	23.41	5.22	0.31		0.01	
Jun 2012	P4	103	82.36	39.55	7.95		0.10	
	P12	164	40.24	4.16	2.12		0.05	
	P20	115	57.84	4.10	0.54		0.01	
	P26	60	49.45	9.28	2.96	6.55	0.06	0.13

BGD

11, 12631–12671, 2014

Estimates of micro-, nano-, and picoplankton contributions to particle export

B. L. Mackinson et al.

Title Page
Abstract | Introduction
Conclusions | References
Tables | Figures
◀◀ | ▶▶
◀ | ▶
Back | Close
Full Screen / Esc
Printer-friendly Version
Interactive Discussion

Table 3. Chl *a* and indicator pigment standing stocks determined by integrating small volume pigment concentrations (determined by HPLC) across the photic zone, pigment fluxes (^{234}Th and PITS-derived) measured at the base of the photic zone, and pigment loss rates, or the percent of the surface concentration represented by those fluxes. Pigment standing stocks are in mg m^{-2} and pigment fluxes are in mg m^{-2} d^{-1}.

Cruise	Station	Depth	Chl *a*	FUCO	PER	HEX	BUT	ALLO	Chl *b*	ZEA
Aug 2010 (2010-14)	P12	Surface (1–75 m)	23.918	3.498	0.375	7.705	1.165	0.220	4.038	1.435
	P16	Surface (1–75 m)	14.165	1.288	0.340	6.010	1.018	0.065	2.588	0.165
	P20	Surface (1–75 m)	19.040	3.138	0.398	6.298	1.453	0.065	2.620	0.188
Feb 2011 (2011-01)	P12	Surface (1–65 m)	30.122	2.848	0.379	5.630	2.431	0.838	7.133	0.922
	P16	Surface (1–95 m)	16.230	1.286	0.202	5.728	1.726	0.161	4.439	1.643
	P20	Surface (1–77 m)	55.053	5.207	0.689	18.064	6.697	1.116	11.435	4.516
Jun 2011 (2011-26)	P4	Surface (1–72 m)	29.791	2.635	0.127	10.619	2.663	0.720	5.836	5.234
	P12	Surface (1–90 m)	26.115	5.060	0.085	11.988	3.263	0.498	2.665	3.063
	P16	Surface (1–105 m)	22.088	4.044	0.104	11.390	2.195	0.181	2.612	1.569
	P20	Surface (1–70 m)	19.421	4.423	0.197	8.132	1.913	0.166	2.090	1.129
	P26	Surface (1–84 m)	29.376	7.239	0.184	10.532	4.406	0.232	3.723	2.663
		Flux at 100 m	0.765	0.474	0.036	0.059	0.0002	0.016	0.028	0.018
		% Flux	2.605	6.548	19.762	0.564	0.004	6.686	0.753	0.658
		Trap (150 m)	0.125	0.056	0.027	0.049	0.014	–	0.017	0.015
		% Flux	0.424	0.767	14.879	0.466	0.311	–	0.461	0.545
Feb 2012 (2012-01)	P4	Surface (1–38 m)	22.684	3.765	–	4.592	1.434	0.917	3.781	0.280
		Flux at 50 m	3.283	1.863		0.811	0.122			
		% Flux	14.471	49.468	–	17.668	8.537	–	–	–
	P12	Surface (1–38 m)	11.003	1.425	0.116	5.606	1.894	0.017	1.915	0.500
		Flux at 100 m	0.046	0.020	0.000	0.014	0.005	0.000	0.000	0.000
		% Flux	0.415	1.381	0.000	0.254	0.249	0.000	0.000	0.000
	P26	Surface (1–38 m)	12.161	2.092	1.218	2.923	1.615	0.137	0.902	0.228
		Flux at 100 m	0.380	0.251	0.035	0.046	0.038	0.000	0.014	0.045
		% Flux	3.126	11.999	2.898	1.581	2.373	0.000	1.524	19.919
Jun 2012 (2012-12)	P4	Surface (1–103 m)	21.313	31.420	–	5.192	–	–	–	–
		Flux at 200 m	1.076	0.919	0.047	0.126	–	–	–	0.036
		% Flux	5.047	2.926	–	2.435	–	–	–	–
	P12	Surface (1–164 m)	27.677	5.967	–	22.445	6.552	–	–	–
		Flux at 200 m	0.051	0.047	–	0.075	0.010	–	0.025	–
		% Flux	0.185	0.787	–	0.335	0.156	–	–	–
	P16	Surface (1–66 m)	12.830	8.722	–	17.321	4.238	–	0.942	0.777
		Flux at 100 m	0.312	0.319	0.045	0.044	0.007	–	–	–
		% Flux	2.431	3.662	–	0.252	0.174	–	–	–
	P20	Surface (1–115 m)	18.344	33.038	–	13.892	–	–	13.090	3.538
		Flux at 100 m	0.016	0.016	0.004	–	0.002	–	0.005	0.001
		% Flux	0.088	0.049	–	–	–	–	0.036	0.033
	P26	Surface (1–60 m)	14.024	1.977	–	13.572	2.018	–	4.969	2.768
		Flux at 100 m	0.255	0.304	–	–	0.029	–	0.025	–
		% Flux	1.821	15.359	–	–	1.437	–	0.507	–
		Trap (100 m)	0.055	0.025	0.006	0.041	0.004	–	0.009	0.008
		% Flux	0.393	1.243	–	0.304	0.190	–	0.179	0.288

Table 4. ^{234}Th and POC fluxes and POC/^{234}Th ratios measured by the PITS traps.

Depth (m)	Days In-situ	^{234}Th flux (dpm m^{-2} d^{-1})	POC flux (mmol m^{-2} d^{-1})	POC/^{234}Th ratio (µmol dpm^{-1})
Jun 2011 P26				
30	3.32	3192 ± 117	15.3 ± 0.4	4.8 ± 0.2
50	3.32	2909 ± 92	10.1 ± 0.3	3.5 ± 0.1
100	3.32	2256 ± 94	5.9 ± 0.2	2.6 ± 0.1
150	3.32	1928 ± 79	5.0 ± 0.2	2.6 ± 0.1
200	3.32	2281 ± 97	8.5 ± 0.3	3.7 ± 0.2
Jun 2012 P26				
30	2.82	3999 ± 206	14.7 ± 0.4	3.7 ± 0.2
50	2.82	5485 ± 290	13.5 ± 0.5	2.5 ± 0.2
100	2.82	3154 ± 192	6.5 ± 0.2	2.1 ± 0.1
150	2.82	2151 ± 135	5.5 ± 0.2	2.5 ± 0.2
200	2.82	3959 ± 129	5.0 ± 0.2	1.3 ± 0.1

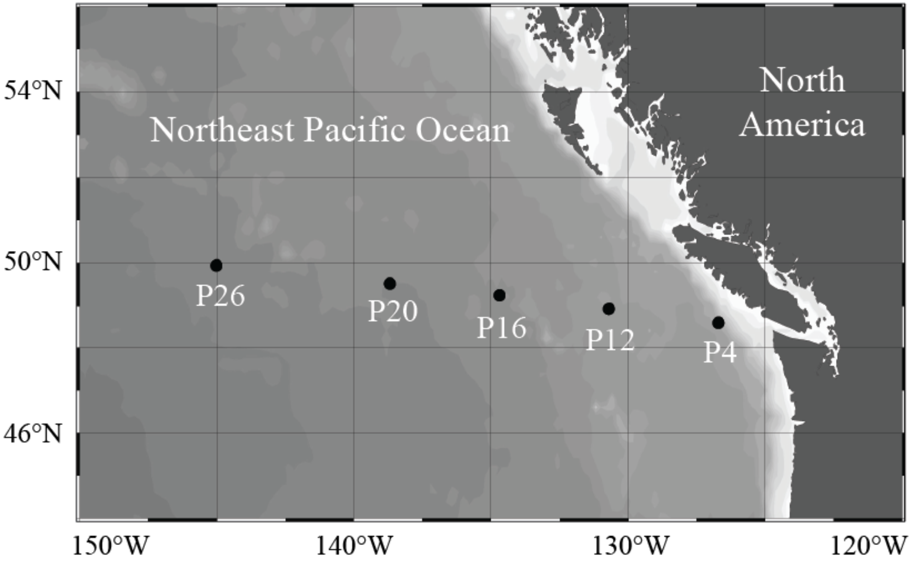

Figure 1. Map showing the Line P stations sampled in this study.

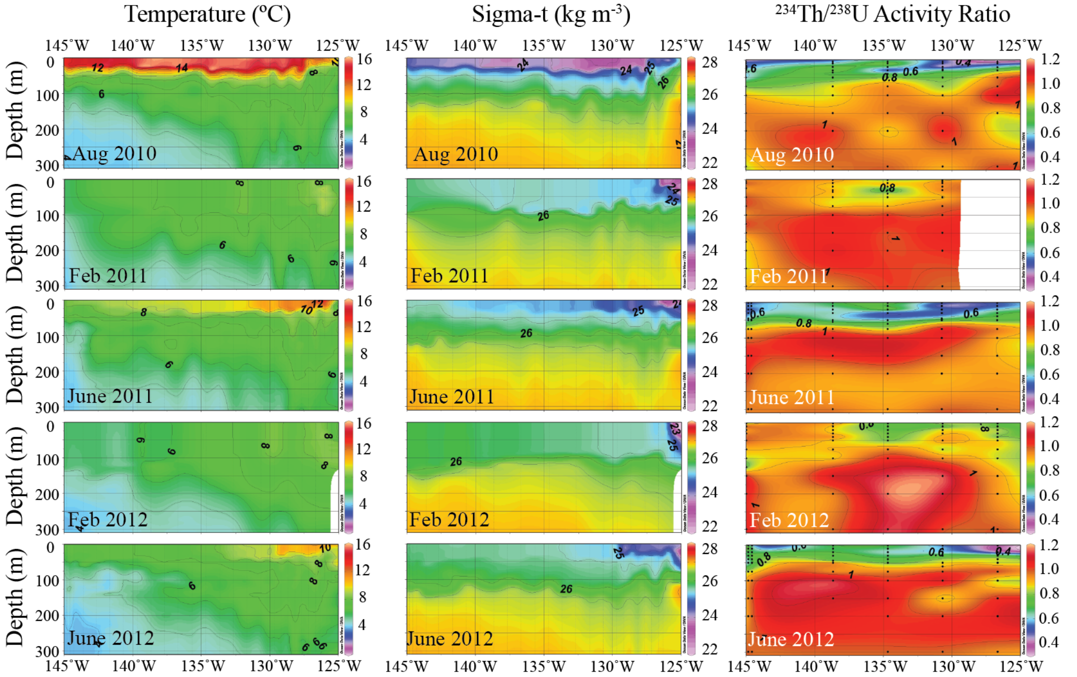

Figure 2. Temperature (°C), Sigma-t ($\mathrm{kg\,m^{-3}}$), and ^{234}Th/^{238}U activity ratio distributions along Line P cruises in August 2010, February 2011, June 2011, February 2012, and June 2012.

BGD
11, 12631–12671, 2014

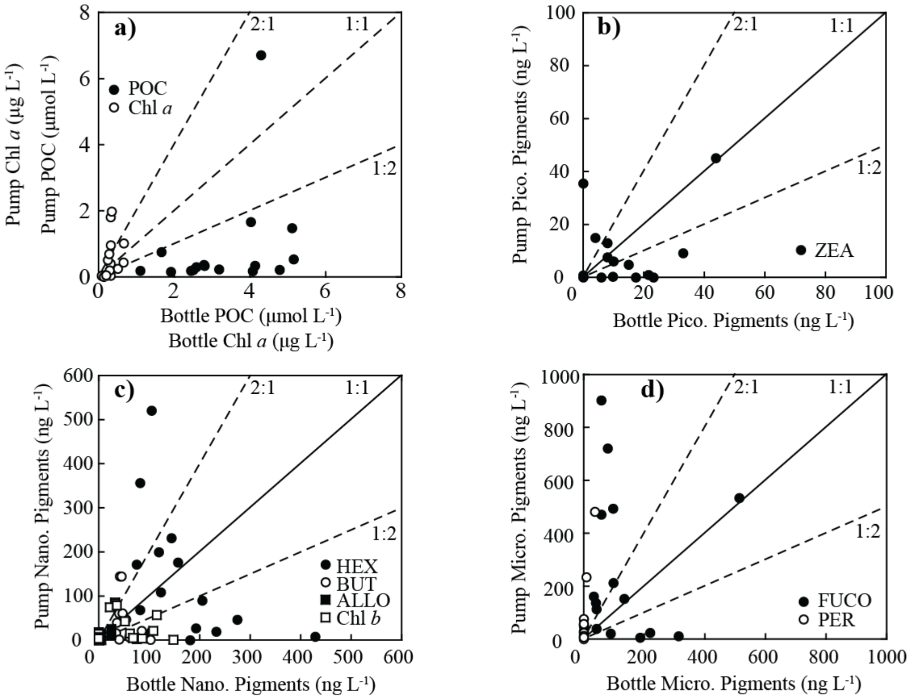

Figure 3. Comparison of small-volume Niskin bottle and large-volume in situ pump measurements of **(a)** POC, **(b)** picoplankton indicator pigments, **(c)** nanoplankton indicator pigments, **(d)** microplankton pigments. Niskin bottle measurements are lower than pump measurements for microplankton pigments, and higher for nanoplankton pigments and POC.

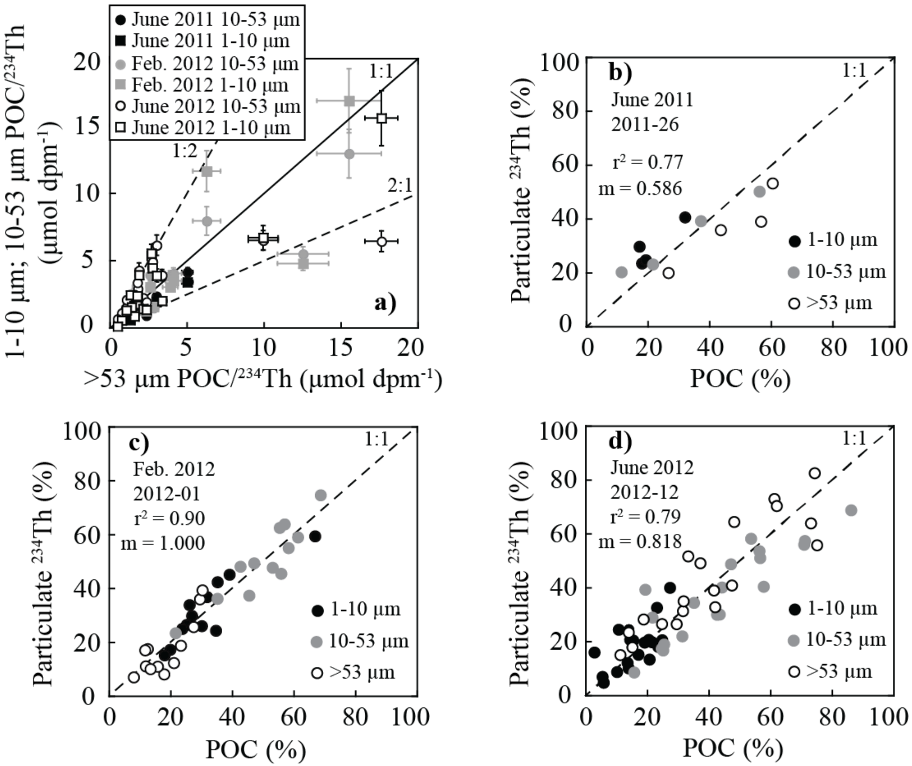

Figure 4. (a) POC/^{234}Th ratios on 1–10 µm particles and on 10–53 µm particles plotted against the POC/^{234}Th ratio on > 53 µm particles. Fractional distributions of POC and particulate ^{234}Th are plotted for three size-classes of particles. The percentage of total POC associated with each particle size-class is plotted against the percentage of total particulate ^{234}Th for samples collected at stations on Line P during **(b)** June 2011, **(c)** February 2012, and **(d)** June 2012. The correlation coefficient (r^2) and the slope of the linear regression (m) are shown for each cruise.

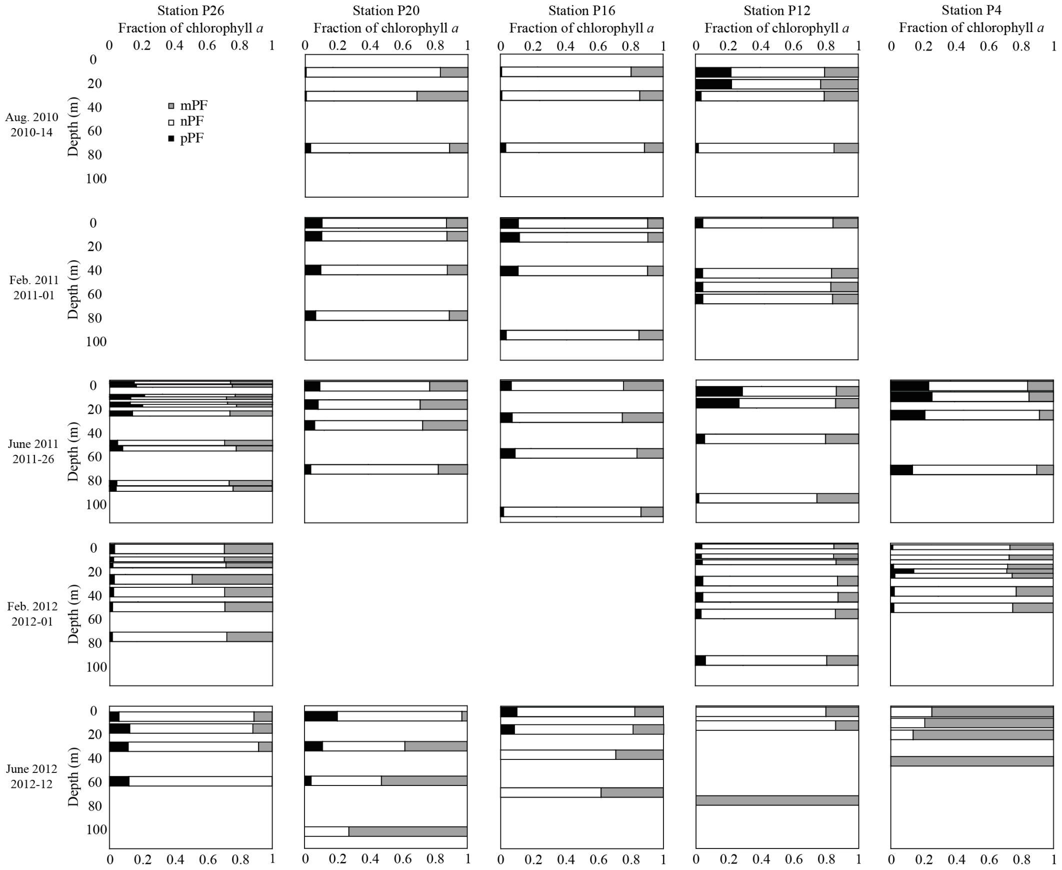

Figure 5. Pigment Proportion Factors (PF) for each phytoplankton size-class plotted as a function of sample depth at stations sampled on Line P during the five cruises in the study. All data were collected from Niskin bottles.

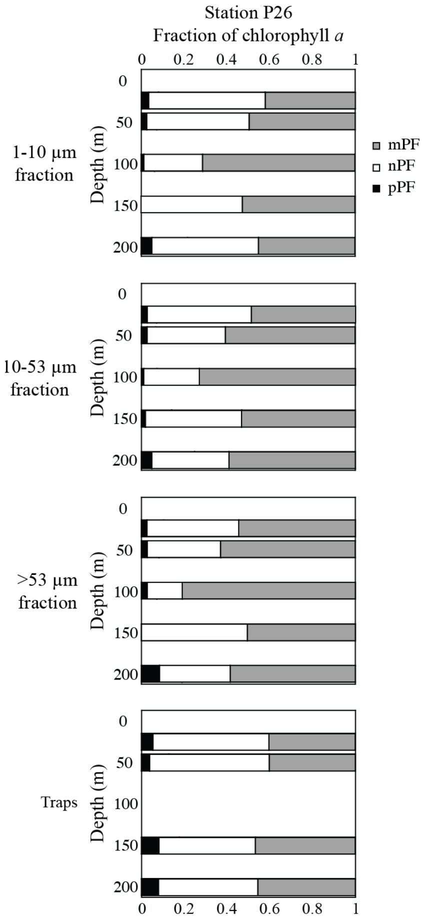

Figure 6. Pigment PF for each phytoplankton size group plotted as a function of sample depth and particle size-class at stations sampled on Line P in June 2011. Size-fractioned data are pump data. Sediment trap PF's are also included.

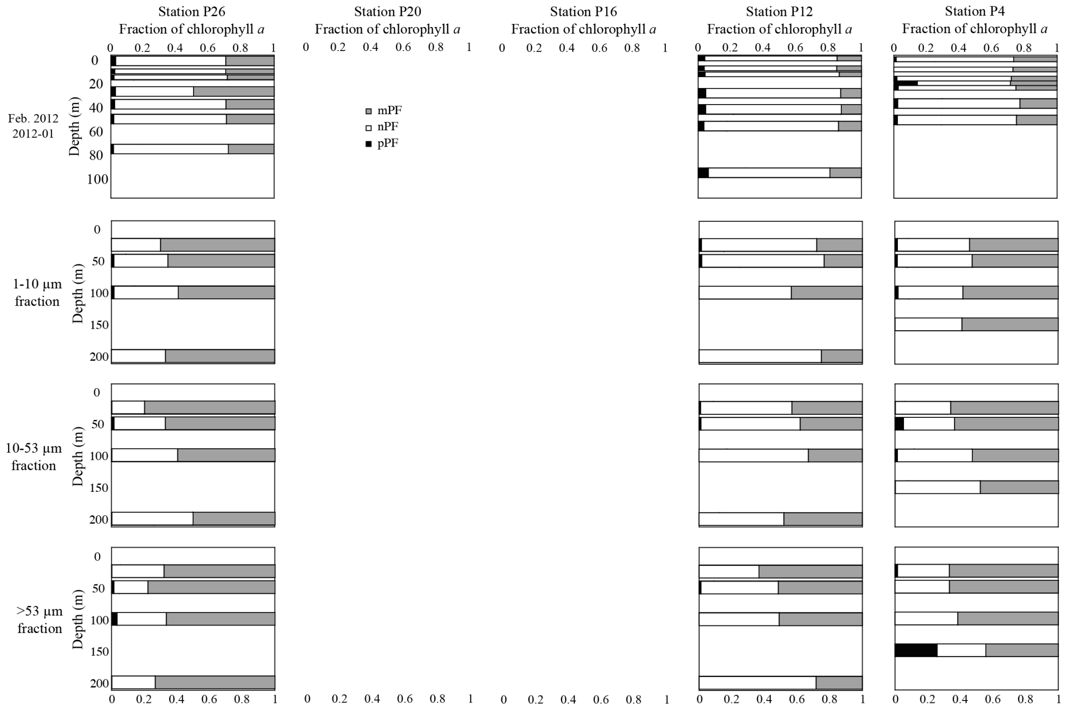

Figure 7. Pigment PF for each phytoplankton size group plotted as a function of sample depth and particle size-class at stations sampled on Line P in February 2012. Size-fractioned data are pump data.

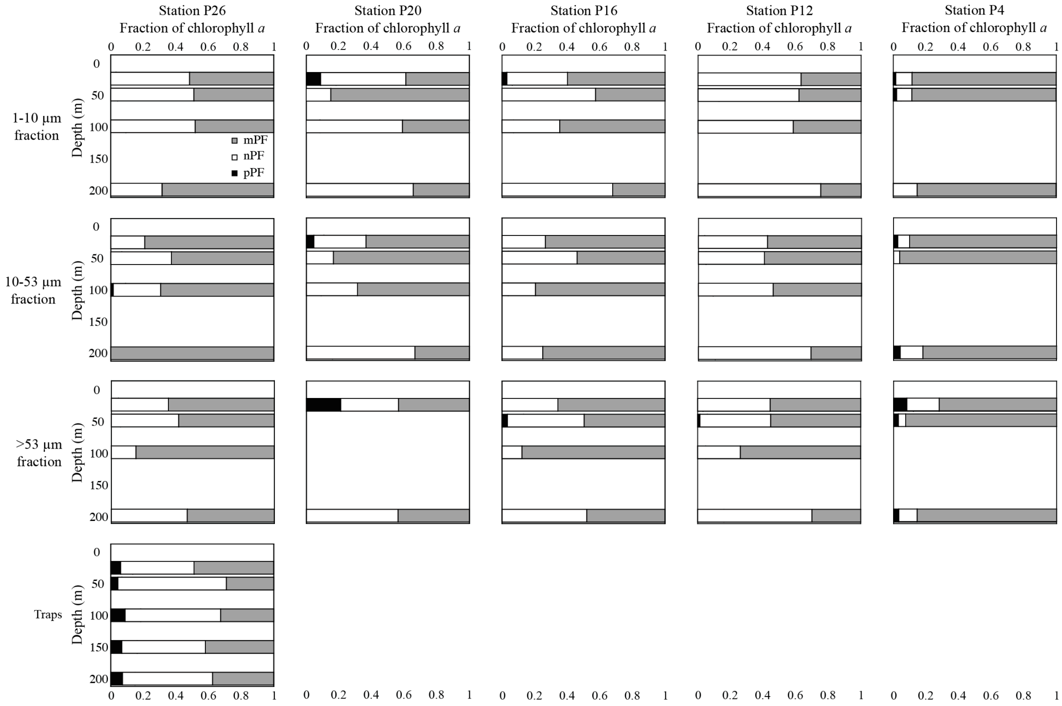

Figure 8. Pigment PF for each phytoplankton size group plotted as a function of sample depth and particle size-class at stations sampled on Line P in June 2012. Size-fractioned data are pump data. Sediment trap PF's are also included where available.

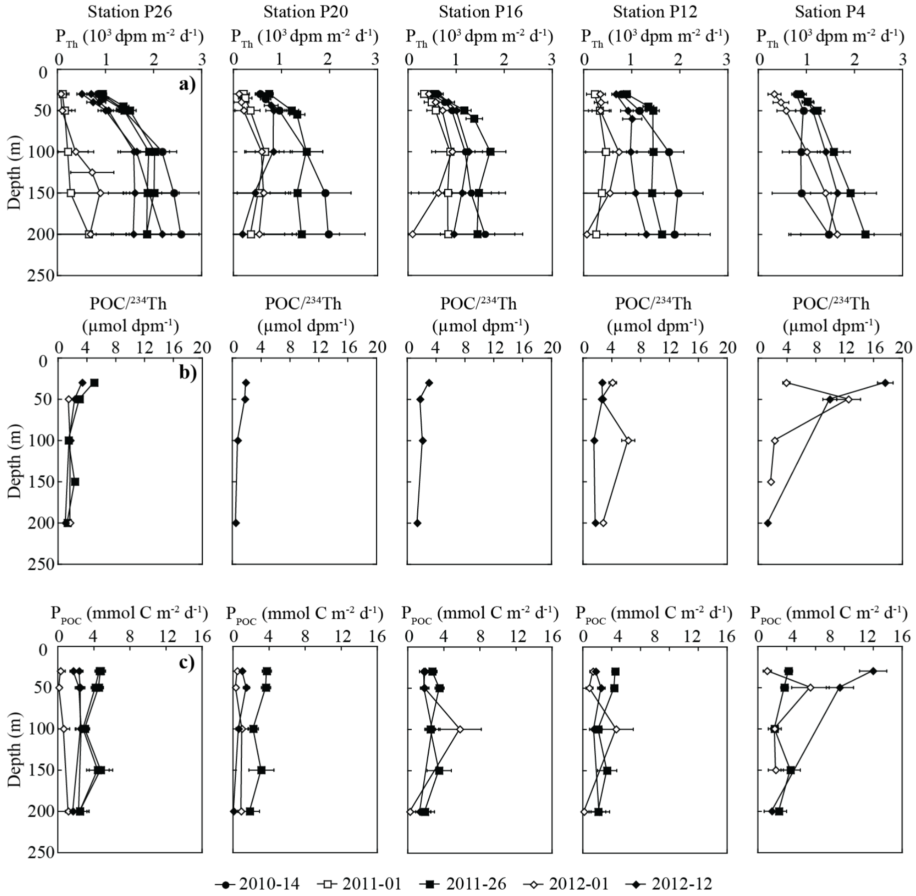

Figure 9. Depth profiles of **(a)** ^{234}Th fluxes (P_{Th}) determined using the 2-D model, **(b)** POC/^{234}Th ratios on > 53 µm particles, and **(c)** ^{234}Th-derived POC fluxes (P_{POC}) at stations on Line P during the five cruises in this study.

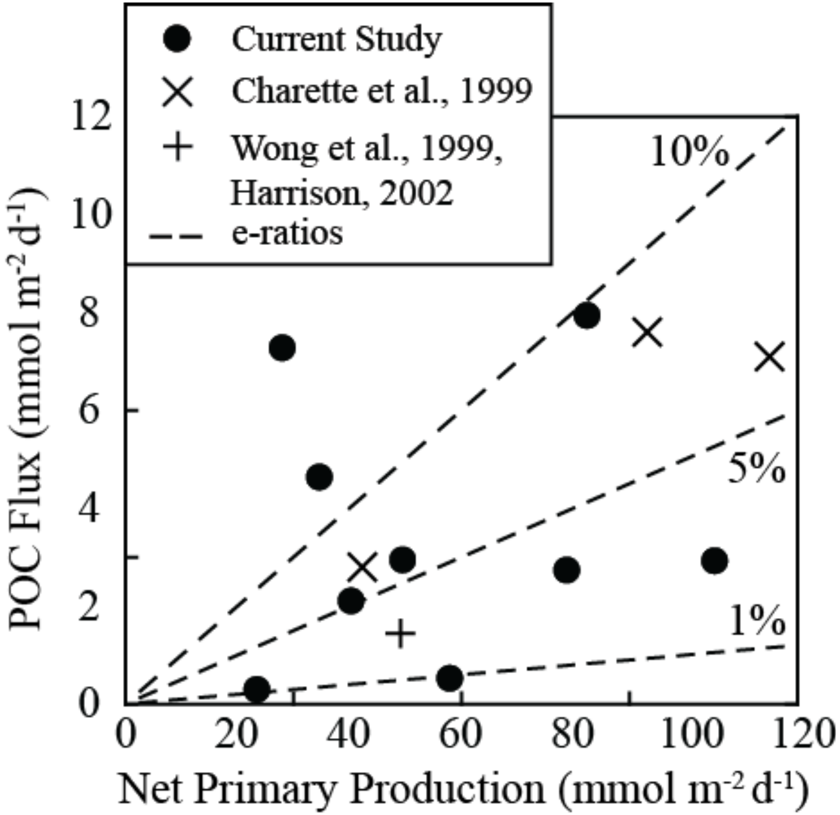

Figure 10. Net primary production (NPP) plotted against ^{234}Th-derived POC fluxes (P_{POC}) for stations along Line P in this study. The slopes of the dashed lines represent ThE-ratios. For reference NPP and P_{POC} values determined by Charette et al. (1999) for winter, spring and summer are included, along with annual average NPP and sediment trap POC fluxes (at 200 m) reported in Harrison (2002) and Wong et al. (1999) respectively.

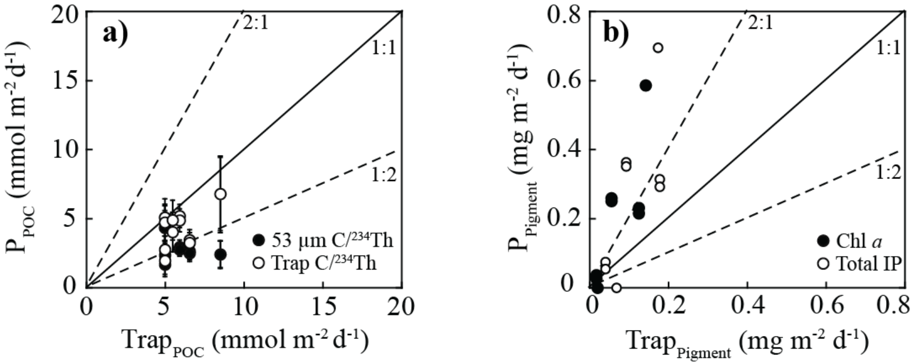

Figure 11. (a) Comparison of sediment trap POC fluxes and ^{234}Th-derived POC fluxes, and **(b)** a comparison of sediment trap Chl *a* and total indicator pigment fluxes and ^{234}Th-derived pigments fluxes at OSP during June 2011 and June 2012.

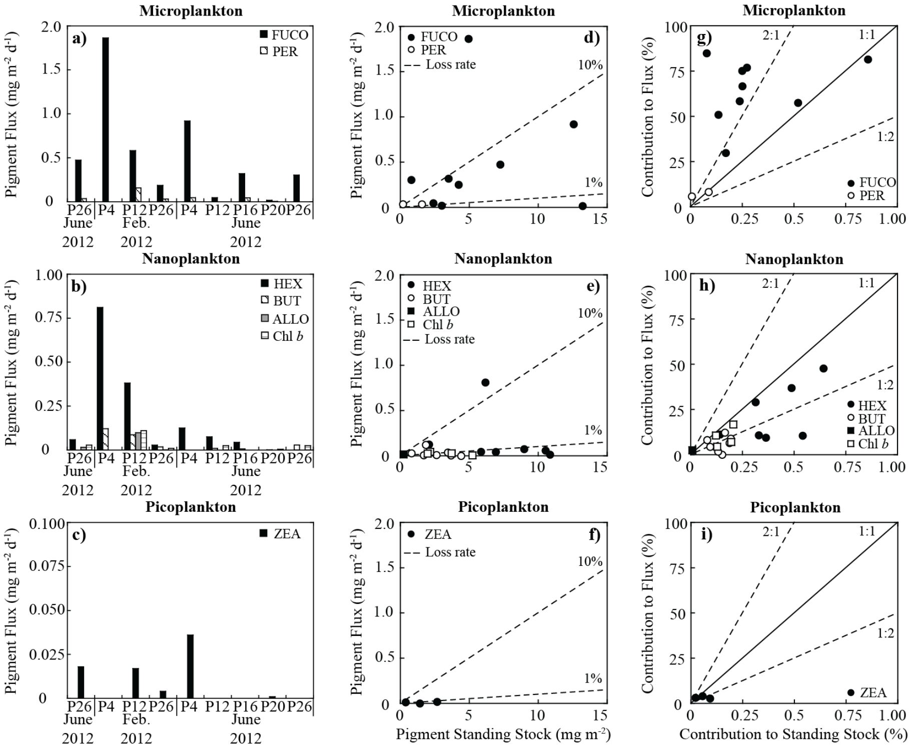

Figure 12. (a–c) ^{234}Th-derived indicator pigment fluxes determined using the Pigment/^{234}Th ratio on > 53 µm particles plotted for micro-, nano-, and picoplankton pigments. **(d–f)** Indicator pigment standing stocks plotted against indicator pigment fluxes for micro-, nano-, and picoplankton pigments. The slopes of the dashed lines indicate pigment loss rates. **(g–i)** The contribution to total pigment standing stock plotted against the contribution to total pigment flux for micro-, nano-, and picoplankton pigments. Data points above the 1 : 1 line indicate preferential export by direct sinking and points below the 1 : 1 line indicate disproportionately low export by direct sinking relative to biomass contributions.